C. von Heynitz, M. Stecker, T. Hofmann and K. Glas

# A Novel Dry Hopping Technology: Kinematic Modelling of a Planetary Rotating Bed Reactor

**Dry hopping can be described as a heterogeneous solid-liquid reaction, calling for high mass transfer rates, low resource consumption, and effective phase separation. This work presents a model-based feasibility analysis of a novel approach to dry hopping that addresses these requirements: the planetary rotating bed reactor (PRBR). This solid-liquid reactor is kinematically enhanced by a planetary gear derivate. The superposition of two rotary motions results in an oscillating acceleration that generates a push-back effect on the hop solids contained in the reactor chamber. Clogging of the retaining filter mesh can thereby be prevented while maintaining high relative flow velocities between hop solids and the circulating beer to promote the desired mass transfer. In this work, a 2D simulation model of the system kinematics is implemented in MATLAB®. The model is governed by a set of analytical equations, allowing for high accuracy and low computational effort. Trajectories and accelerations of relevant reactor segments are calculated, considering design and process variables like gear diameter and rotation speed of the input shafts. The existence of the underlying push-back effect and its technical viability are verified and evaluated by appropriate performance indicators in consideration of the fluid throughput. As a result, the PRBR promises to be a fast, hop-saving and fully scalable solution for dry hopping and other heterogeneous reactions.**

Descriptors: dry hopping, heterogeneous reaction, mass transfer, kinematics, rotating bed reactor, filtration

## 1 Introduction

With its unique flavour and aroma profile, dry hopping has become widely established in the brewing industry over the last years. During dry hopping, hop cones or pellets are brought into contact with the beer in order to extract different aroma components. Due to the low temperatures of 1 to 20 °C this is known as cold extraction [1].

The typical hop aroma in beer is mainly caused by volatile hop oils, accounting for 0,5 – 3 % of the dry matter of hops [2]. The oil consists of hydrocarbons (mainly terpenes and aliphatic hydrocarbons), oxygenated hydrocarbons (mainly terpenoids like geraniol or linalool) and sulphur compounds [3, 4]. This variety of ingredients leads to the distinct hop aroma intensity in beer and especially in dry hopped beers [5].

### 1.1 Dry hopping from a process engineering perspective

The extraction rate of hop volatiles is influenced by multiple factors like process type [6], tank geometry and scale [7], beer temperature [8], particle size distribution of hop solids [9], varietal differences of hops [10] and yeasts biotransformations [11]. Furthermore, the contact time and reaction surface of the hop solids are of critical importance to the external mass transfer of flavour compounds since low process temperature limits the diffusion rate. At present, there is no unified method for dry hopping [6]. Likewise, there is very little literature on respective process technologies. However, one can distinguish between static and dynamic extraction. Static extraction refers to the placing of hops in the storage tank without high technical effort [12]. The deposition of insoluble hop components in beer can be prevented by using fine-mesh bags, however this reduces extraction efficiency [12]. Moreover, in static extraction the temporal decrease of local concentration gradients increases the process time to a few days [13]. Dynamic extraction approaches aim to enhance the mass transfer, e.g. by pre-dissolving pellets in beer or water and then pumping them into the tank [12, 13]. Alternatively, pellets are shot into the beer by $CO_2$ overpressure for quick dissolution [14]. Again, in most continuous processes, pellets are placed in an external $CO_2$ pressurized tank being percolated by the beer. This setup allows to supress oxygenation but also calls for the removal of the finely distributed particles afterwards [6, 12].

From a process engineering perspective dry hopping can be described as a heterogeneous solid–liquid reaction that is strongly aided by convective flow of the fluid. To increase the external mass transfer rate one can maximize the reaction surface by using smaller hop particles and provide a high relative velocity between the particles and the beer. Basically, there are two processual approaches for heterogeneous reactions: the stirred reactor (STR) and the (rotating) fixed-bed reactor (FBR) [15]. In an STR, the phases are mixed or evenly distributed in the liquid

https://doi.org/10.23763/BrSc20-09heynitz

**Authors**

Christian von Heynitz, Manuel Stecker, Thomas Hofmann, Karl Glas, Chair of Food Chemistry and Molecular Sensory Science, Technical University of Munich, Freising, Germany; corresponding author: c.heynitz@tum.de

phase while in the FBR, the solids are encapsulated in a reaction chamber and transited by the reaction medium. The STR allows the use of smaller particles, yet facing the challenge of the following solid–liquid separation. Moreover, the particles tend to move along with the stirring flow resulting in low relative velocities. In contrast, in an FBR a higher relative velocity can be achieved. However, smaller particles will cause a dense filter cake, lower flow velocities, increased pressure drop and as a result reduced mass transfer [16]. Hop pellets are comprised of small and deformable particles, which form an unfavourable cake with very poor hydraulic properties leading to mesh or filter clogging. Hence, dry hopping exhibits a particular need for a device providing high convective flow while coping with small and unstable solids. At this point we introduce the planetary rotating bed reactor (PRBR) for considerably increased mass transfer.

### 1.2 Description of the PRBR

The PRBR consists of multiple rotating bed reactors mounted to a respective number of gearwheels, representing the planets of a modified planetary gear. Figure 1 shows a virtual 3D model of an exemplary setup containing three planet gearwheels (green) and therefore three reactor chambers. These reactor chambers are comprised of an outer perforated wall which retains a filter mesh, as well as top and bottom walls with fluid inlets [15]. The sun gearwheel (orange) and the planetary carrier (blue) are rotated by respective drive units (not shown). The mechanical power is transmitted by two shafts whereby the first sun-shaft (orange) is born within the hollow shaft of the planetary carrier (blue). The coordination of both rotational speeds allows the well-defined adjustment of the planet gearwheels, and therefore reactor chambers, motions. Hence, every reactor chamber experiences a rotation around its own axis, as well as the rotation around the principal axis defined by the central sun shaft. This resembles the manner the earth rotates around the sun. The two centripetal accelerations arising from the two rotary motions can be combined in a way that their total vector sum forms an acceleration vector which periodically changes its direction relative to the centre of the chamber.

For dry hopping this effect can be exploited as follows: the reactor chambers, that each are divided in circular sector shaped compartments by radial barriers, are filled with hops. This loading process can take place manually or automatically via fluid transport. The whole device is submerged in the beer meant to be hopped. After the sun and the planetary carrier have started to spin with their assigned angular velocities, two effects come into operation. Due to the rotation around its own axis each reactor chamber functions like a centrifugal pump, conveying the beer radially outwards through the bed of hops. This creates suction within the chamber such that beer is drawn in through the top and bottom inlets, resulting in continuous percolation (see Fig. 1). This percolation also allows automatic loading of hops into the chamber; hops are simply added to the tank, then flushed into the reactor chamber and trapped by the filter mesh. The oscillating acceleration described earlier provides a push-back effect on hop particles at the mesh surface of the outer reactor wall. They are thereby lifted from the reactor wall periodically, resulting in disruption of the filter cake and prevention of clogging by the fine and deformable hop particles. This maintains a high flow rate of

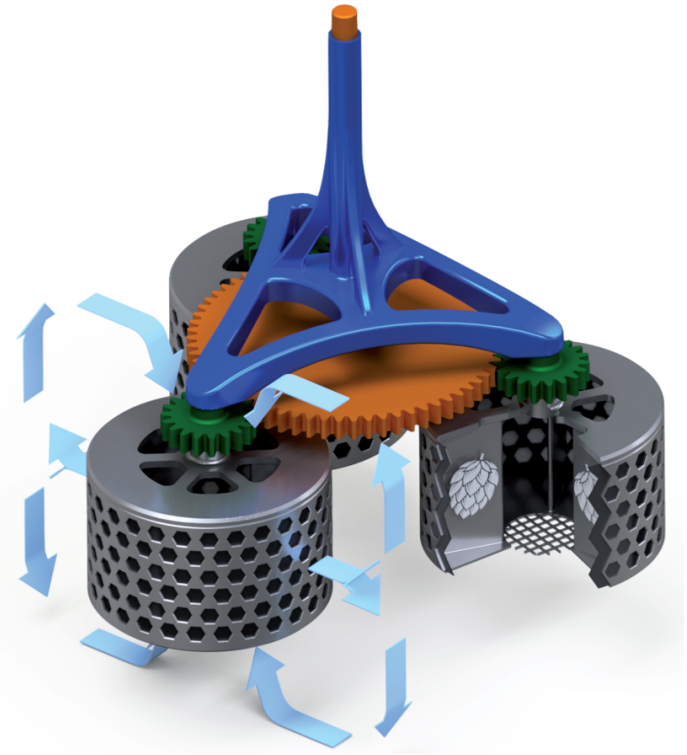

**Fig. 1 Virtual 3D model of the planetary rotating bed reactor (PRBR) with insight into the reactor chamber and indicated flow pattern**

beer through the reactor compartments. By enforcing high relative velocities between hops and beer the external mass transfer rate of sensory relevant substances is promoted.

In this work we implemented a 2D simulation model of the system kinematics to perform a feasibility analysis regarding the PRBR and its underlying push-back effect on particles at the mesh surface. The model is governed by a set of analytical motion equations, allowing for high accuracy and low computational effort. The trajectory and acceleration components of a representative point $P$ on the inner peripheral wall of the reactor chamber are calculated to evaluate the mechanical interaction between the hops and the reactor wall (filter mesh). The extent of the push-back effect as well as a relative measure for the beer through-put are considered with respect to crucial design and process variables like gear diameter and rotation speed of the input shafts. Dimensionless assessment parameters were applied where possible in the simulation setup to generate scalable results.

## 2 Materials and methods

In this section we discuss the methodological framework of the kinematic simulation model carried out in the present study. Kinematics denote the mathematical description of motions by means of geometric quantities leaving the effecting forces and torques unconsidered. After a generic description of the underlying geometric architecture and nomenclature, we present a forward model of the system and use it to predict the kinematics of one defined configuration. The model is then extended with the introduction of a nested loop routine to calculate and compare the performance of different parameter configurations. Finally, the set parameter

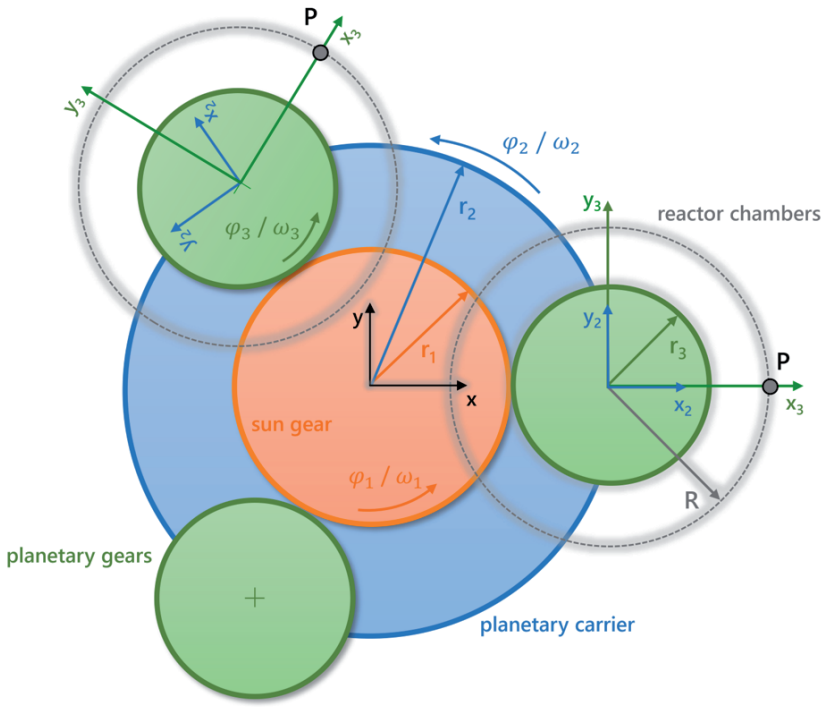


**Fig. 2** **Model sketch as 2D top view projection of the PRBR, showing the three rotational subsystems with their respective coordinate systems (frames) including the relevant geometric and kinematic quantities**

values, and the software packages and functions applied, as well as the reasoning behind these selections, are presented.

## 2.1 System and parameter identification

Before designing and implementing a mathematical description, we first identify the relevant design- and process parameters, required coordinates as well as the respective system boundaries. Focussing on the planetary gear drive as the functional core of the system we can identify three rotational subsystems as shown in figure 2: the central sun gearwheel (orange, #1), the coaxial planetary carrier (blue, #2), the planet gearwheels (green, #3) co-rotating with the reactor chambers (grey, #3). At this point we also introduce the respective body-fixed coordinate systems (1–3) from now on denoted as frames. Furthermore, we define an inertial coordinate system (black) referred to as the global frame, which is centered on the main rotation axis and not subject to any agitation.

As a spatial reference spot for the subsequent modelling process, we set the point *P*, located at the intersection between the x-axis of the body fixed planet ($x_3$) and the chamber wall. That way, the crucial mechanical interaction between the chamber wall and the hops can be investigated. Table 1 gives an overview of all design and process parameters introduced in figure 2, consisting of geometric dimensions as well as rotation angles and their respective angular velocities.

For the purpose of this study, it is negligible whether the three planets shown in figure 2 are interpreted as three different planets or one particular planet in different positions. Due to the discrete rotational symmetry of the system, all planets can be expected to show the same kinematic behaviour, regardless of how many of them are present.

**Table 1** **Overview of system parameters referring to Figure 2**

| | |
|---|---|
| **Design parameters** | |
| $r_1$ | Effective radius of sun gearwheel |
| $r_2$ | Radius of planetary carrier circle radius of reactor axis trajectory |
| $r_3$ | Effective radius of planet gearwheels (planets) |
| $R$ | Radius of reactor chamber |
| **Process parameters** | |
| $\varphi_1$ | Rotation angle of sun gearwheel |
| $\varphi_2$ | Rotation angle of planetary carrier |
| $\varphi_3$ | Rotation angle of planet gearwheel relative to planetary carrier |
| $\omega_1$ | Angular velocity of sun gearwheel |
| $\omega_2$ | Angular velocity of planetary carrier |
| $\omega_3$ | Angular velocity of planet gearwheels relative to planetary carrier |

## 2.2 Constitution of the forward model

In this section, we derive the kinematic equations required to simulate the motion of all subsystems, particularly the reactor chamber represented by point $P$. Since we have identified three rotational systems driven by two input shafts and therefore two degrees of freedom, there must be one kinematic constraint between those rotations. This constraint can be identified at the point of interaction between the sun gear and the planet, where both tangential velocities match due to teeth engagement:

$$v_1(r_1) = v_{3,abs}(r_3)$$

$v_1(r_1)$ can be found via

$$v_1(r_1) = \omega_1 r_1$$

while for $v_{3,abs}$, we take that $\omega_3$ is defined as being relative to the planetary system. Taking the correct rotational directions into account, it follows that

$$v_{3,abs}(r_3) = \omega_2 r_1 - \omega_3 r_3$$

which describes the superposition of the speed induced by the planetary carrier and the own rotation of the planet. Thereby we can derive the constraint in question, namely

$$\omega_3 = r_1 \frac{\omega_2 - \omega_1}{r_2 - r_1}$$

In order to quantify and evaluate the push-back effect on the hop solids, it is necessary to properly model the accelerations occurring

at point $P$. The position vector of $P$ in cartesian coordinates with respect to the global frame is given by

$$\mathbf{r}_{OP}(\varphi_2, \varphi_3) = \begin{pmatrix} x_P \\ y_P \end{pmatrix} = \begin{pmatrix} r_2 \cos\varphi_2 + R\cos(\varphi_2 + \varphi_3) \\ r_2 \sin\varphi_2 + R\sin(\varphi_2 + \varphi_3) \end{pmatrix}$$

Since we investigate a stationary-state process, for constant angular velocities $d\omega_i/dt = 0$, time dependency can be added for temporal differentiation by

$$\mathbf{r}_{OP}(t) = \begin{pmatrix} r_2 \cos(\omega_2 t) + R\cos\big((\omega_2 + \omega_3)t\big) \\ r_2 \sin(\omega_2 t) + R\sin\big((\omega_2 + \omega_3)t\big) \end{pmatrix}$$

The second time derivative leads to the acceleration vector of $P$

$$\boldsymbol{a}_P(t) = \begin{pmatrix} a_{x,P} \\ a_{y,P} \end{pmatrix} = \frac{d^2\mathbf{r}}{dt^2} = \begin{pmatrix} -{\omega_2}^2 r_2 \cos(\omega_2 t) - R\cos\big(t\,(\omega_2 + \omega_3)\big)(\omega_2 + \omega_3)^2 \\ -{\omega_2}^2 r_2 \sin(\omega_2 t) - R\sin\big(t\,(\omega_2 + \omega_3)\big)(\omega_2 + \omega_3)^2 \end{pmatrix}$$

Now for both the position and acceleration vector the explicit time can be eliminated again by substituting the time $t = \varphi_3/\omega_3$ to make the model a function of the angle $\varphi_3$, which is the parameter representing one full revolution of the reactor relative to the planetary carrier.

$$\mathbf{r}_{OP}(\varphi_3) = \begin{pmatrix} r_2 \cos\left(\frac{\omega_2\varphi_3}{\omega_3}\right) + R\cos\left(\frac{\varphi_3(\omega_2 + \omega_3)}{\omega_3}\right) \\ R\sin\left(\frac{\varphi_3(\omega_2 + \omega_3)}{\omega_3}\right) + r_2 \sin\left(\frac{\omega_2\varphi_3}{\omega_3}\right) \end{pmatrix}$$

$$\mathbf{a}_P(\varphi_3) = \begin{pmatrix} -{\omega_2}^2 r_2 \cos\left(\frac{\omega_2\varphi_3}{\omega_3}\right) - R\cos\left(\frac{\varphi_3(\omega_2 + \omega_3)}{\omega_3}\right)(\omega_2 + \omega_3)^2 \\ -{\omega_2}^2 r_2 \sin\left(\frac{\omega_2\varphi_3}{\omega_3}\right) - R\sin\left(\frac{\varphi_3(\omega_2 + \omega_3)}{\omega_3}\right)(\omega_2 + \omega_3)^2 \end{pmatrix}$$

Note that for $\omega_3 = 0$, a division by zero is created, however this does not hinder the algorithm, since this case is not a feasible setting regarding the push-back effect. The acceleration vector of P in the global frame needs to be transformed into the body-fixed reactor frame RF by multiplication with the respective rotational matrices.

$$\mathbf{R}_{\varphi_3}(\varphi_3) = \begin{bmatrix} \cos(\varphi_3) & \sin(\varphi_3) \\ -\sin(\varphi_3) & \cos(\varphi_3) \end{bmatrix} \quad \mathbf{R}_{\varphi_2}(\varphi_3) = \begin{bmatrix} \cos\left(\frac{\omega_2\varphi_3}{\omega_3}\right) & \sin\left(\frac{\omega_2\varphi_3}{\omega_3}\right) \\ -\sin\left(\frac{\omega_2\varphi_3}{\omega_3}\right) & \cos\left(\frac{\omega_2\varphi_3}{\omega_3}\right) \end{bmatrix}$$

$$\mathbf{a}_P^{RF}(\varphi_3) = \mathbf{R}_{\varphi_3}(\varphi_3)\mathbf{R}_{\varphi_2}(\varphi_3)\mathbf{a}_P(\varphi_3)$$

The x-component of this acceleration $a_{x,P}^{RF}$ is isolated, since it describes the radial component of the acceleration concerning P within the reactor frame (see Fig. 2). By expressing the ratio between the maximum and minimum acceleration as below, we derive a dimensionless measure which holds solely when the two accelerations have different signs. Therefore, the presence of the push-back effect can be validated or invalidated for a given configuration, while expressing its magnitude as a relative quantity.

$$PBE = \frac{\max\left(a_{x,P}^{RF}\right)}{\min\left(a_{x,P}^{RF}\right)}\left(0{,}5\ \mathrm{sgn}\left(\frac{\max\left(a_{x,P}^{RF}\right)}{\min\left(a_{x,P}^{RF}\right)}\right) - 0{,}5\right)$$

In addition to the description of the push-back effect, a sufficient convective flow of beer must also be ensured. Although an absolute quantification of the fluid throughput is not possible with the present model, we can identify the absolute angular velocity of the reactor as a proportional quantity to describe the flowrate in a relative sense. It can be determined by

$$\omega_{3,abs} = \omega_2 + \omega_3$$

To provide a dimensionless performance indicator, considering both the magnitude of the push-back effect as well as the implied convective flow, we introduce $\eta$, defined as

$$\eta = PBE\,\frac{|\omega_{3,abs}|}{\sqrt{|\omega_1\omega_2|}}$$

In accordance with the scalable approach of this work we further declare two dimensionless quantities representing the design- and process parameters as simulation input. The rpm ratio describes that of the rotation speed of the two input shafts (planet carrier and sun) and is given by:

$$\xi_\omega = \frac{\omega_2}{\omega_1}$$

The gear ratio describes that of the diameters of the planets and the sun gear and is given by:

$$\xi_g = \frac{r_1}{r_3}$$

The input-output structure of all model variables is listed in table 2.

**Table 2 Overview of the forward model parameters**

| | |
|---|---|
| **Input: Fixed model parameters** | |
| $r_2$=1 | Planetary carrier radius |
| $\omega_1$=–1 | Angular velocity of sun gear |
| $R$=$\alpha r_2$=0,7 | Radius of reactor chamber |
| **Input: Variable model parameters** | |
| $\xi_\omega$ | Rpm ratio |
| $\xi_g$ | Gear ratio |
| **Input: Simulation parameters** | |
| $\varphi_{3,start}$ | Lower bound of $\varphi_3$ |
| $\varphi_{3,end}$ | Upper bound of $\varphi_3$ |
| $n_{sim}$ | Number of discrete simulation steps |
| **Calculated auxiliary parameters** | |
| $\omega_3$ | Relative angular velocity of planet gearwheel / reactor |
| $r_3$ | Effective radius of planet gearwheel |
| $r_1$ | Effective radius of sun gearwheel |
| **Output parameters** | |
| $\omega_{3,abs}$ | Angular velocity of planet gearwheel / reactor relative to global frame |
| $PBE$ | Push-back effect index |
| $\mathbf{r}_{OP}(\varphi_3)$ | Position coordinates of point P in global frame |
| $\mathbf{a}_P(\varphi_3)$ | Acceleration vector of P in global frame with respect to $\varphi_3$ |
| $a_P(\varphi_3)$ | Acceleration vector of P in reactor frame with respect to $\varphi_3$ |
| $\eta$ | Overall performance index |

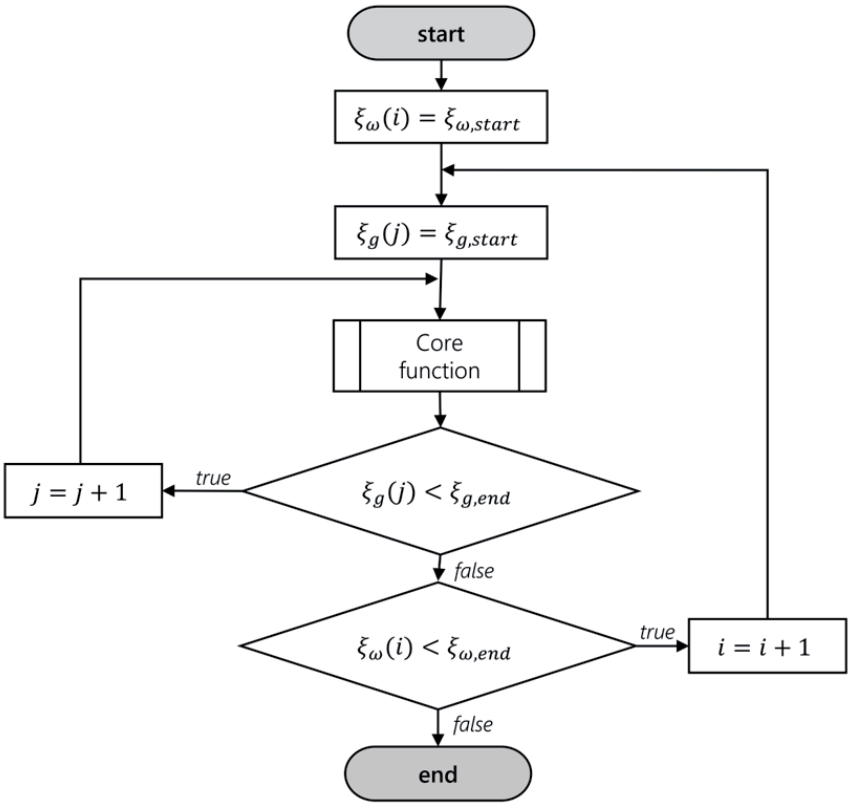


**Fig. 3 Program flow chart of the nested loop routine, looping over rpm ratio and gear ratio**

The main simulation parameter $\varphi_3$ is defined by a lower and upper bound as well as the number of discrete steps in between. This is appropriate, since for $\varphi_3$ equidistant spacing is applied. The forward model generates a video-file containing an animation of the rotating system including point $P$ with its respective acceleration vectors. For easier scalability, the planetary carrier radius is set to one and the angular velocity of the sun gear to minus one. The radius of the reactor chamber is set to 0,7 as a compromise between high containing volume and high flow rates on the one hand and enough space between the reactor chambers on the other.

## 2.3 Constitution of the nested loop model

In order to generate and investigate a cluster of different solutions based on a given range of input parameters we implemented an additional routine containing a nested loop. The loop parameters are the rpm ratio $\xi_\omega$ (outer loop) and the gear ratio $\xi_g$ (inner loop). The structure of the routine is shown as program flow chart in figure 3.

The nested loop allows the calculation of the push-back effect $PBE$, the global reactor speed $\omega_{3,abs}$ and the overall performance indicator $\eta$ as functions of rpm ratio and gear ratio to assess different combinations of design and process setups. The additional parameters required for this routine are listed in table 3.

## 2.4 Parameter setting / assignment

After introducing all parameters relevant for the model, we now can assign them with values for the aspired simulation of this study. These are listed in table 4.

Since the model relies on analytical relations, the step size does not influence the precision of the results through numerical deviations e.g. by time integration. Therefore, the step sizes are chosen to deliver data for smooth visualization. Basically, the parameter setting of the forward model also applies for the nested loop since the same core function as in the forward model is called. Due to the looping, rpm ratio and gear ratio are each defined as vectors, thus the forward parameters $\xi_\omega$ and $\xi_g$ are obsolete for the nested loop. Due to the low computational effort and the insignificant calculation times, their ranges can be broad to evaluate the full spectrum of possible solutions.

## 2.5 Simulation software and functions

The simulation is implemented in MathWorks MATLAB® Version R2020a and consists of two script files, one for the forward model and another one for the nested loop. Both call the same core function file delivering the calculated values for position and acceleration at point $P$. Another Live Script is dedicated to the symbolic time differentiation of the position vector for gathering the acceleration equations as introduced before plus the coordinate transformation in terms of the rotational matrices. The following toolboxes and non-standard functions were used:

**Table 3 Additional simulation parameters for the nested loop model**

| | |
|---|---|
| **Input: simulation parameters** | |
| $\xi_{\omega,start}$ | Lower bound rpm ratio |
| $\xi_{\omega,end}$ | Upper bound rpm ratio |
| $n[\xi_\omega]$ | Number of discretization steps for rpm ratio |
| $\xi_{g,start}$ | Lower bound gear ratio |
| $\xi_{g,end}$ | Upper bound gear ratio |
| $n[\xi_g]$ | Number of discretization steps for gear ratio |
| **Output parameters as functions of rpm- and gear ratio** | |
| $\omega_{3,abs}(\xi_\omega,\xi_g)$ | Absolute reactor rpm |
| $PBE(\xi_\omega,\xi_g)$ | Push-back effect index |
| $\eta(\xi_\omega,\xi_g)$ | Overall performance index |

**Table 4 Selected parameter setting for the present study**

| Both models | Forward model | Nested loop model |
|---|---|---|
| $\varphi_{3,start} = 0$ | $\xi_\omega = 0{,}95$ | $\xi_{\omega,start} = 0{,}01$ |
| $\varphi_{3,end} = 2\pi$ | $\xi_g = 8$ | $\xi_{\omega,end} = 0{,}98$ |
| $n_{sim} = 1000$ | | $n[\xi_\omega] = 2500$ |
| | | $\xi_{g,start} = 0{,}1$ |
| | | $\xi_{g,end} = 10$ |
| | | $n[\xi_g] = 2500$ |

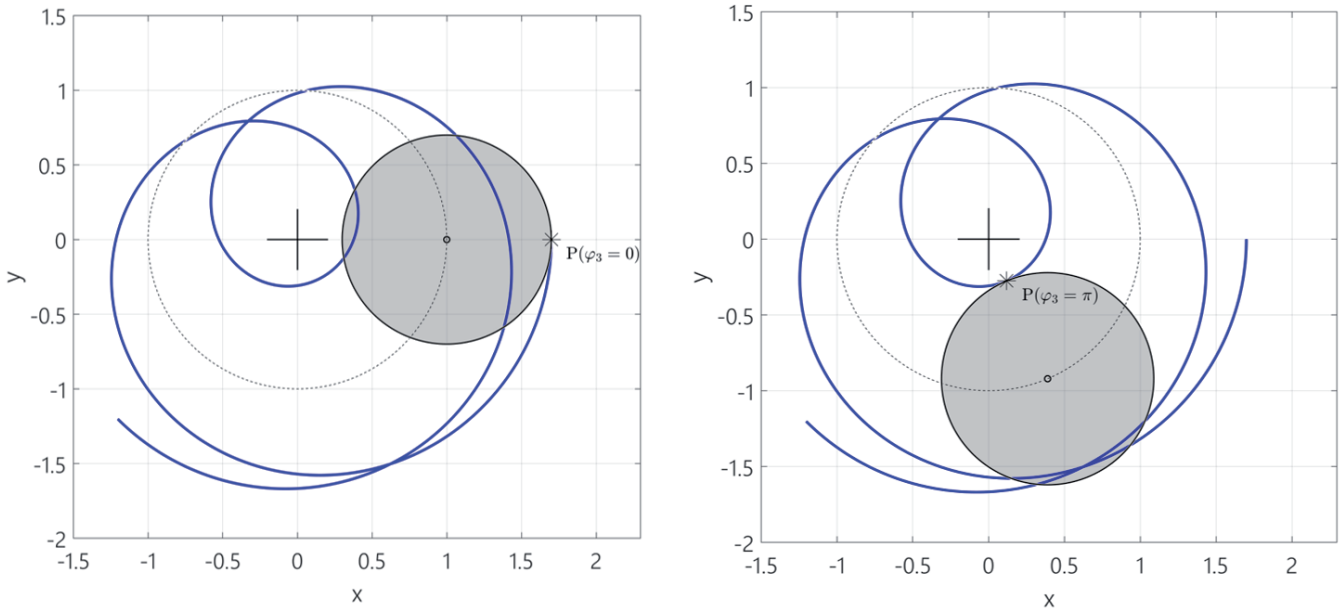


**Fig. 4 Global trajectory of point $P$ (blue) with respective reactor poses at $\varphi_3 = 0$ (left) and $\varphi_3 = \pi$ (right) for $\xi_\omega = 0{,}95$ / $\xi_g = 8$ / $R = 0{,}7$**

- Symbolic Math Toolbox® for analytical derivation of governing equations
- Image Processing Toolbox® to draw scale independent circles in the animation
- Function *arrow.m from Matlab file exchange server* to draw decent acceleration vectors
- Function *filledCircle.m from Matlab file exchange server* to draw circles with filled area

## 3 Results and discussion

All calculations and therefore all results refer to the prior defined point $P$ as representative geometric location due to the given rotational symmetries of the system. First, we will discuss the results of one single forward simulation run with the defined set of input parameters. This includes both the 2D-trajectory as well as the acceleration characteristics of the reactor. To assess the behaviour and performance of different design and process setups, the results of the nested loop model are shown and discussed considering the push-back effect and the reactor`s absolute rotational speed as relative index for the conveyed through-put. Finally, we transfer the findings to a technical implementation example.

### 3.1 Forward model

The forward model covers the reactor kinematics for one representative revolution relative to the planetary carrier.

$$\varphi_3 \in [\,0\,;2\,\pi\,[$$

The calculated output data refers to a rpm ratio of $\xi_\omega = 0{,}95$, a gear ratio of $\xi_g = 8$ and a reactor radius $R = 0{,}7$. (see Table 4)

#### *3.1.1 Global trajectory of point $P$*

For a better understanding and evaluation of the system kinematics, the 2D-trajectory of point $P$ has been calculated with respect to the spatial pose of the reactor chamber and within the global frame. Figure 4 shows that trajectory for two decisive simulation steps combined with the respective reactor positions: the first step, where $\varphi_3 = 0$ as well as an in between step which exactly describes half of a representative revolution ($\varphi_3 = \pi$) of the reactor. Regarding figure 2 the revolution starts with the planetary frame and reactor frame being aligned and therefor point $P$ at the radial outbound position. We observe, that for both steps the trajectory (blue) runs tangentially to the reactor edge at P, already allowing the conclusion that the resulting acceleration vector of $P$ is perpendicular to the reactor edge, consisting therefore only of a radial component within a body-fixed reactor frame. This is because at both steps point $P$ does not move towards or away from the rotation axis of the planetary carrier and thereby no Coriolis acceleration can be induced. An even more important finding for the purpose of the PRBR concept is the counter-oriented curvature of the trajectory

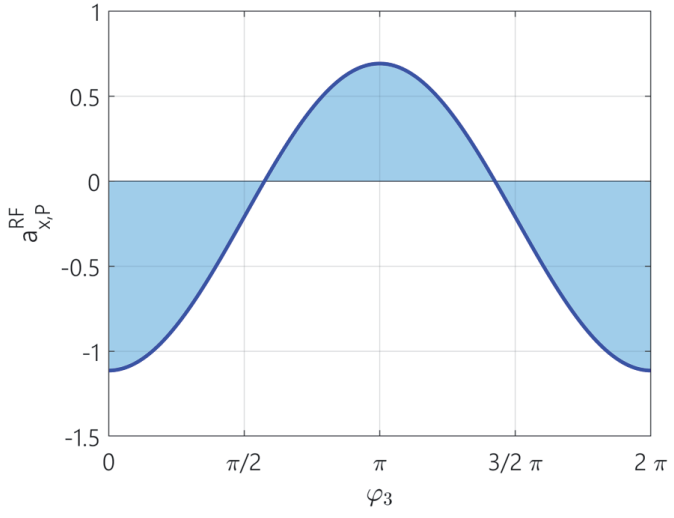


**Fig. 5 Radial acceleration component in $P$ within reactor frame over angle $\varphi_3$ for $\xi_\omega = 0{,}95$ / $\xi_g = 8$ / $R = 0{,}7$**

relative to the reactor at $\varphi_3 = \pi$ in comparison with the initial position $\varphi_3 = 0$. This suggests that it is de-facto possible to configure the system parameters for a directional change of the resulting acceleration (push-back effect) at P observing from the reactor chamber.

### *3.1.2 Acceleration of point P*

Figure 5 indicates that the radial acceleration of point $P$ with respect to the reactor displays a sinusoidal characteristic over a representative revolution. The oscillation occurs between a positive maximum and a negative minimum, whose ratio defines the PBE as introduced before. The absolute value of the positive maximum acceleration is smaller than the absolute value of the negative minimum. This makes sense, since at $\varphi_3 = 0$ the two rotary movements of the planetary carrier and the planet/reactor each cause an equal oriented overlap and therefor summation of their centripetal accelerations and in contrast a subtractive overlap at $\varphi_3 = \pi$. We further observe, that during one cycle the period of positive acceleration is shorter than the negative one. This is expected to be favourable since the negative one delivers the driving force for the fluid pumping through the reaction chambers and the positive one the counter force for the push-back of the hop particles away from the mesh of the chamber wall.

Figure 6 shows 12 rotational reactor poses of one full cycle typified by the respective positions of P relative to the planetary carrier and thereby according to $\varphi_3$. The circular area corresponds to the reactor`s top surface. The acceleration vectors relatively oriented to the planetary carrier are plotted for each position of P. Positions $\varphi_3 = 0$ and $\varphi_3 = \pi$ exhibit solely radial acceleration components, while in all other positions there is an additional tangential component observing from the reactor frame. One might wonder, if the line extensions of the vectors are crossing each other in one certain point within the planetary carrier frame. We found that this is the

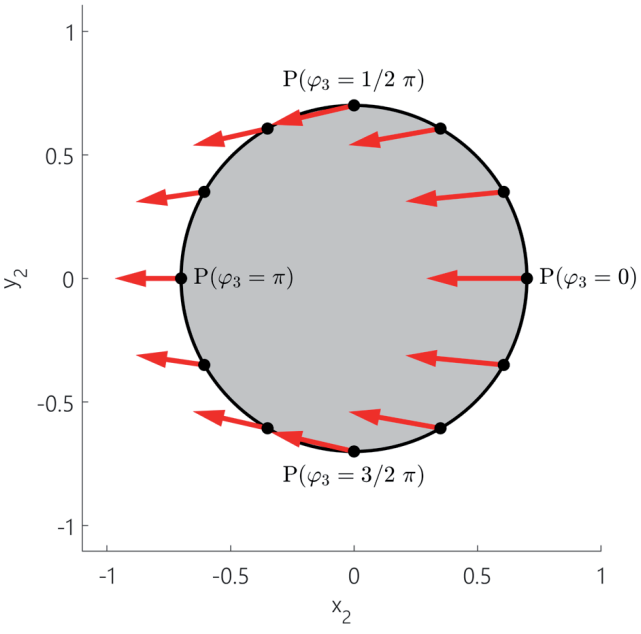


**Fig. 6 Acceleration vector in point $P$ for different rotational reactor poses $\varphi_3$, displayed in the planetary carrier frame**

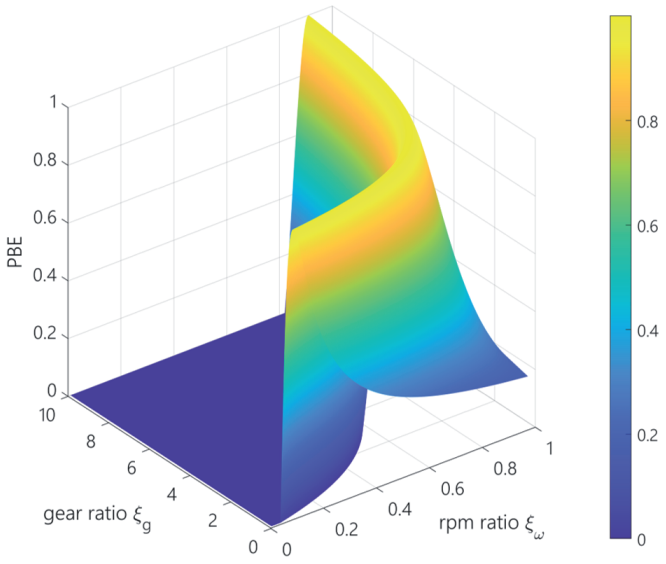


**Fig. 7 PBE with respect to rpm- and gear ratio**

case, although this point does not match the main rotation axis (origin of global frame). Remember that this figure or rather its axis refer to the frame of the planetary carrier. Hence, the point of crossing is moving along a circle within the global frame underlining the occurrence of Coriolis accelerations, additionally to the centripetal accelerations.

### *3.1.3 PBE and performance indicator*

As shown in the last section, for the given setup we obtain a positive maximum acceleration of $a_{x,P}^{RF}$ = 0,69 and a negative minimum acceleration of $a_{x,P}^{RF}$ = -1,11, by definition, leading to a push-back effect of $PBE$ = 0,62. The reactor`s absolute (relative to global frame) angular velocity is $\omega_{3,abs}$ = 0,55. This results in a performance indicator of $\eta$ = 0,33. At this point we may solely conclude that there is a significant push-back effect regarding the directional change of accelerations. The numerical assessment is dependent from the comparison of different configurations as carried out in the following sections.

## 3.2 Nested loop model

### *3.2.1 Push-back effect*

Turning to the nested loop model we first consider the push-back effect $PBE$ with respect to the rpm- and gear ratio as shown in figure 7. We observe a curved ridge of maxima with $PBE$ being equal to one. For increasing gear ratios this ridge approximates asymptotically the rpm ratio of one. This is reasonable, since for $\xi_\omega$ = 1 the planetary carrier and the sun system each spin at same speed leading thereby to a relative angular velocity of zero regarding the planets. In this case the reactor and thereby point $P$ display no movement relative to the planetary carrier and as a result no push-back effect is possible. Proceeding from the ridge towards higher gear ratios and lower rpm ratios we find a plane of $PBE$ being equal to zero. These setups do not show a directional change of the acceleration vector in P and hence are algebraically sort out (set to zero) as defined in section 2.

Beyond $\xi_\omega = 1$ there is no further rise of $PBE$ to be found for higher rpm ratios. We conclude, that for a given process a particular or a minimum required value of $PBE$ lies within a limited range of parameter combinations regarding rpm- and gear ratio. Fortunately, this range appears to be technically feasible with respect to the design limits of gearwheel pairs as well as electric engine setups.

### *3.2.2 Global rotational speed*

In order to add a factual value to the process, it is crucial to likewise ensure an appropriate magnitude of flow rate. Latter can be assessed by determining the reactor`s angular velocity with respect to the global frame $\omega_{3,abs}$. Figure 8 considers $\omega_{3,abs}$ with respect to rpm- and gear ratio. For better illustration, the plane given by $\omega_{3,abs} = 0$ is highlighted in transparent grey. We found that the line of intersection (highlighted red) between this plane and the function $\omega_{3,abs}$ ($\xi_\omega$, $\xi_g$ ) – constituting all the setups with no global rector rotation – has the same course as the ridge of the $PBE$ maxima in figure 7. By setting $\omega_{3,abs} = 0$ we identified the regarding equation as follows:

$$\xi_\omega = \frac{\xi_g}{1 + \xi_g}$$

We concluded that maximizing $PBE$ and $\omega_{3,abs}$ is to some extent mutual exclusive. At first view, that might seem unfavourable, but one should also consider the relative duration of the acceleration periods described before. Higher $PBE$ comes with partially shorter periods of “pumping” accelerations within one cycle compared to the push-back periods. However, at this point we are not yet able to evaluate the impact of this factor on the real process.

### *3.2.3 Overall performance indicator η*

To provide a framework for further analysis as well as a best guess from the current perspective and state of investigation we introduced $\eta$ as overall performance indicator. Figure 9 shows $\eta$ as a function of our design- and process parameters $\xi_\omega$ and $\xi_g$. The calculated structure confirms our earlier conclusion of oppositeness

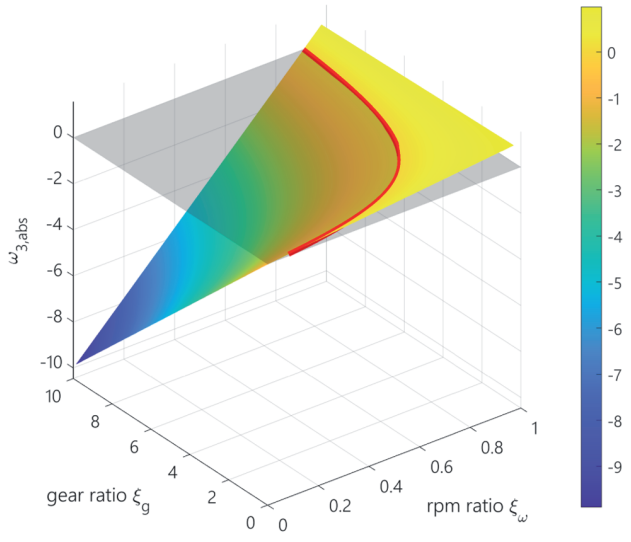


**Fig. 8 Reactor‘s angular velocity relative to the global frame and with respect to rpm- and gear ratio**

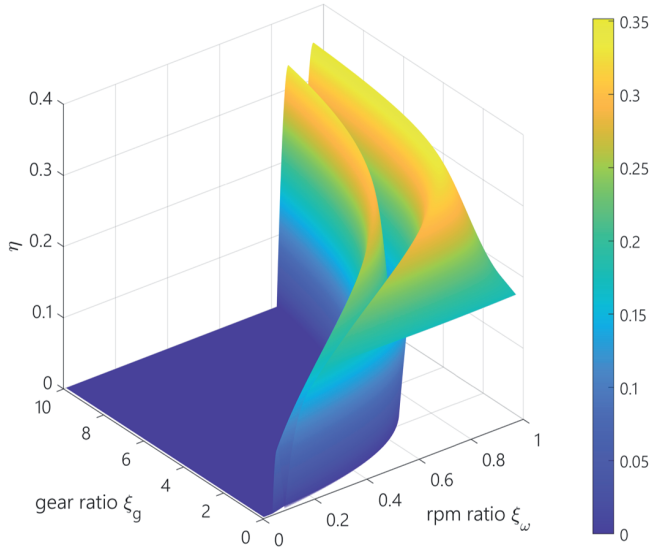


**Fig. 9 Performance indicator $\eta$ with respect to rpm- and gear ratio**

regarding $PBE$ and $\omega_{3,abs}$. Instead of one ridge like with the $PBE$ in figure 7 we find two of them separated by a canyon following the course of the prior ridge. The ridge towards higher rpm ratios exhibits slightly higher values for $\eta$ and represents positive values of $\omega_{3,abs}$ while the other one is characterized by setups leading to a counter oriented reactor rotation. In summary higher gear ratios and rpm ratios close to one seem favourable in terms of $\eta$. We also conclude that there are setups allowing for simultaneously taking advantage of the push-back effect and a significant global rotation of the reactor for fluid transport.

## 3.3 Technical implementation

In this section, we embed the previous findings in a simplified parametric design process and thus arrive at a concrete design example. Let us assume, we already have the empiric knowledge to quantify the geometric dimensions and number of reactor chambers required for a particular dry hopping process, mainly defined by a given batch size of beer and its properties. Therefore, the radius of the reactor chamber is known as $R = 100$ mm.

1. The known radius $R$ implies a possible range of global reactor speeds. According to state-of-the-art reactors we thereby choose $\omega_{3,abs} = 200$ rpm

2. From $R$ we also can derive the radius of the planetary carrier from the known relation $r_2 = \frac{R}{\alpha}$. Using $\alpha = 0{,}7$ we obtain $r_2 = 143$ mm

3. Empirical findings also allow to determine the desired magnitude of the push-back effect $PBE$. We choose $PBE = 0{,}62$ and obtain a characteristic implicit numerical function $f(\xi_\omega, \xi_g) = 0$ from the simulation model defined by the projection of the respective isoline on the $PBE$ surface.

4. The model is now used as an optimization routine to iteratively find absolute design- and process values along $f(\xi_\omega, \xi_g) = 0$ while also fulfilling the condition $\omega_{3,abs} = 200$ rpm. This leads

to $r_1$ = 127 mm, $r_3$ = 16 mm, $\omega_1$ = 364 rpm and $\omega_2$ = 345 rpm

Among this dimensioning, the design can be further extended. One of the key advantages of the PRBR is the combination of heterogeneous reaction and filtration in one device. To enhance the filtration function, at least one of the chambers can be equipped with a finer membrane in place of the filter mesh. This would ensure that even small particles that get into the beer are separated.

Furthermore, flow baffles can be mounted to the sun system (radially outside of the reactor chambers) to decrease the rotational movement of the beer and thereby to increase the flow rate. This construction element makes use of the two given rotational subsystems at different speeds.

## 4 Summary and conclusions

In this contribution, we presented a feasibility analysis regarding use of a planetary rotating bed reactor (PRBR) as novel technology for dry hopping. The PRBR consists of a rotating solid-liquid reactor kinematically enhanced by a planetary gear derivate generating a push-back effect to prevent hop clogging of the peripheral filter mesh. This effect is based on the superposition of two rotary motions and thereby a directional change of the acting accelerations. We introduced a 2D simulation framework to model the kinematics of the PRBR, implemented in MATLAB®. Therewith we proved the existence of the underlying push-back effect and reached a better understanding for the acceleration behaviour at the contact interface between the hop solids and the reactor. The model allowed us to verify the technical viability as well as to quantify the sensitivity of the system to the selected process variables. With the approach of dimensionless parametrization, we demonstrated that the kinematic concept of the PRBR holds in all scales.

The PRBR promises to be a fast, hop-saving and fully scalable technology for dry hopping and other heterogeneous reactions, since it combines efficient mass transfer and filtration in one device. In future we aim to further develop this concept together with broad-minded industry partners. Based on the findings of the present work the next step should be the design of a prototype for experimental investigation on the process. This would allow the quantification of extraction efficiency as well as the degree of solid retention with respect to the generated flow rates. Furthermore, the process behaviour regarding oxygen input and foam formation are to be addressed. The gathered experimental data will help to extend and optimize the present simulation model.

### Acknowledgements

Concerning the presented technology, the Technical University of Munich has filed a European patent as well as a PCT application, both published on 24.06.2020 under: EP3669976A1. The licence agency in charge is Bayerische Patentallianz GmbH.

## 5 References

1. Engstle, J.; Kuhn, M.; Kohles, M.; Briesen, H. and Först, P.: Disintegration of hop pellets during dry hopping, BrewingScience, **69** (2016), no. 11-12, pp. 123-127.
2. Keukeleire, D. de: Fundamentals of beer and hop chemistry, Química Nova, **23** (2000), no. 1, pp. 108-112.
3. Schönberger, C. and Kostelecky, T.: 125th Anniversary Review: The Role of Hops in Brewing, Journal of the Institute of Brewing, **117** (2011), no. 3, pp. 259-267.
4. Hauser, D. G.; Lafontaine, S. R. and Shellhammer, T. H.: Extraction Efficiency of Dry-Hopping, Journal of the American Society of Brewing Chemists, **77** (2019), no. 3, pp. 188-198.
5. Lafontaine, S. R.; Vollmer, D. M.; Shellhammer, T. H. and Pereira, C. B.: The effectiveness of hop volatile markers for forecasting dry-hop aroma intensity and quality of cascade and centennial hops, BrewingScience, **71** (2018), no. 11-12, pp. 116-140.
6. Wolfe, P. H.: A study of factors affecting the extraction of flavor when dry hopping beer, Masters Thesis, Oregon State University.
7. Schnaitter, M.; Kell, A.; Kollmannsberger, H.; Schüll, F.; Gastl, M. and Becker, T.: Scale-up of Dry Hopping Trials: Importance of Scale for Aroma and Taste Perceptions, Chemie Ingenieur Technik, **88** (2016), no. 12, pp. 1955-1965.
8. Oladokun, O.; James, S.; Cowley, T.; Smart, K.; Hort, J. and Cook, D.: Dry-Hopping: The effects of temperature and hop variety on the bittering profiles and properties of resultant beers, BrewingScience, **70** (2017), no. 11-12, pp. 187-196.
9. Bandelt Riess, P. M.; Engstle, J. and Först, P.: Characterizing the filtration behavior of hop particles for efficient dry hopping methods, BrewingScience, **71** (2018), no. 9-10, pp. 74-80.
10. Takoi, K.; Tokita, K.; Sanekata, A.; Usami, Y.; Itoga, Y.; Koie, K. et al.: Varietal difference of hop-derived flavour compounds in late-hopped/dry-hopped beers, BrewingScience, **69** (2016), no. 1-2, pp. 1-7.
11. Takoi, K.; Koie, K.; Itoga, Y.; Katayama, Y.; Shimase, M.; Nakayama, Y. et al.: Biotransformation of hop-derived monoterpene alcohols by lager yeast and their contribution to the flavor of hopped beer, Journal of agricultural and food chemistry, **58** (2010), no. 8, pp. 5050-5058.
12. Mitter, W. and Cocuzza, S.: Wiederbelebtes Verfahren, Brauindustrie, **4** (2012), no. 4, pp. 10-12.
13. Lafontaine, S. R. and Shellhammer, T. H.: Impact of static dry-hopping rate on the sensory and analytical profiles of beer, Journal of the Institute of Brewing, **124** (2018), no. 4, pp. 434-442.
14. Schönberger C. and Wiesen E.: Die Kunst der Kalthopfung, Der Doemensianer, **1** (2013), pp. 42-43.
15. Maurilio Magosso: Investigation Of The Spinchem® Rotating Bed Reactor: Internally And Externally Mass Transfer Limited Reactions, Tesi di Laurea Magistrale, Università Degli Studi Di Padova, 2015.
16. Pär Alapää: Remediation of Contaminated Groundwater Using a SpinChem Rotating Bed Reactor, Luleå University of Technology, 2018.

*Received 4 May 2020, accepted 2 June 2020*